FOURTEENTH EUROPEAN ROTORCRAFT FORUM

Paper No. 8.6

A STUDY OF THE INFLUENCE OF A HELICOPTER ROTOR BLADE ON THE FOLLOWING BLADES USING EULER EQUATIONS

E. Krämer, J. Hertel, S. Wagner

Universität der Bundeswehr München

Institut für Luftfahrttechnik und Leichtbau

September 20–23, 1988

MILANO, ITALY

ASSOCIAZIONE INDUSTRIE AEROSPAZIALI

ASSOCIAZIONE ITALIANA DI AERONAUTICA ED ASTRONAUTICA

A STUDY OF THE INFLUENCE OF A HELICOPTER ROTOR BLADE ON THE FOLLOWING BLADES USING EULER EQUATIONS

Ewald Krämer Johann Hertel
Research Assistants

Siegfried Wagner
Professor

Institut für Luftfahrttechnik und Leichtbau
Universität der Bundeswehr München
Neubiberg, W. Germany

ABSTRACT

An Euler procedure for the calculation of sub- and transonic flow around multi-bladed helicopter rotors is presented. The procedure shows that the Euler equations themselves are very well suited to describe the vortex transport correctly, if certain requirements were met. Therefore, they represent proper means to comprehend the main problem of steady rotor flow, the complex blade-vortex-interaction, without utilizing external vortex models.

Results are presented which agree well with measurements from the model rotor of Caradonna and Tung, and which reproduce the effects that grid topology and the distance of the far-field boundaries show on vortex convection.

NOTATIONS

AR	- aspect ratio
c	- chord length
C_p	- local pressure coefficient related to local dynamic pressure
C_{p_a}	- pressure coefficient related to sound dynamic pressure
D	- Jacobian determinant
e	- total energy per unit volume
$\bar{e}$	- roenergy
$\vec{E},\vec{F},\vec{G}$	- flux vectors
H	- total enthalpy per unit mass
h	- rothalpy
$\vec{J}$	- right-hand-side vector
M_{tip}	- tip Mach number
p	- static pressure
r	- local radial position
R	- rotor radius
q	- absolute value of velocity
t	- time direction
$\vec{v}=(u,v,w)^T$	- velocity vector

X,Y,Z	- cartesian or cylindrical coordinates respectively
x,y,z	- cartesian coordinates
φ,r,z	- cylindrical coordinates
θ_c	- collective pitch angle
ρ	- density
κ	- ratio of specific heats
ξ,η,ζ	- curvilinear coordinates
Ψ	- azimuth angle
$\vec{\Phi}$	- conservative solution vector
$\vec{\omega} = (0,0,\Omega)^T$	- angular velocity of the coordinate frame

1. INTRODUCTION

Since considerable times Euler procedures have become indispensable tools for the construction of fixed wings or even complete aircraft configurations, for the estimation of engine compressors and turbines, as well as for the aerodynamic design of motorcar shapes.
Moreover, intensive research is persued in developing Navier-Stokes procedures at least for simple geometries for industrial application.

In the area of helicopter design, however, the development of adaptable Euler procedures is at its beginning, especially in Europe, not to mention Navier-Stokes procedures. This is astonishing all the more as highly sophisticated numerical methods are required to exploit the very small possibilities of performance enhancement profitably. In the USA successful research results have been presented for a few years [1-8]. On the European side, with few exceptions [9,10] which also publications of the present work belong to, hardly activities are known.

Potential procedures of various exactness levels, used up to now, show quite useful results, combined with small storage and calculation requirements. However, especially when realizing transonic effects within the blade tip region, and/or the wake and the tip vortex, insufficiencies appear which must be partially corrected via coupling with external models, partly based on empiric results [13-25].

On the other hand, using Euler procedures it is possible to reproduce the main flow phenomena which are generated by helicopter rotor blades, except viscous effects.
In particular, they have the ability to treat rotational, anisentropic flows and to correctly transport the rotation brought into the flow region. This permits their application to the airflow around a rotor blade which is significantly influenced by the interference with the tip vortices of the preceeding blades. Therefore, it is possible to reach a correct determination of the airloads and the resulting aerodynamic, flight mechanical, and acoustic characteristics.

These fundamental capabilities of the Euler equations are limited in the numerical application by two severe impairments: Not only artificial viscosity which must be involved within the algorithms in order to comply with numerical stability requirements, but also discretization errors, extremely apparent in the region of coarse grid structures, are responsible for a diffusion of the tip vortex. Furthermore, a great dependence upon the formulation of the far-field boundary conditions is shown, especially for vortex descent and contraction.

The present work shall make a contribution to producing a high leveled procedure for industrial application in aerodynamic helicopter design in Europe, as they are already commonly used in the U.S.A.

The procedure presented is an alternative to those which eliminate the

described deficiencies by coupling with an external wake model.
Rather, the attempt is made to widely avoid such a proceeding by the following means: First, by applying an algorithm based on the EUFLEX-code of A. Eberle [28] which distinguishes itself by a low numerical viscosity. Secondly, by application of locally refined grids and, finally, by employing non-reflecting conditions at the far-field boundaries which have to be rather far distant from the rotor blade.

For the employment of the computational grids two different approaches were used: In one case, a cylinder was selected which involves the complete rotor disk including the wake, and whose grid lines are arranged in an 0-0-structure. Its advantage of covering a large physical region by a small number of grid points is reduced by the presence of very large grid cells in certain areas along the vortex path.
Exactly reversed are the conditions using the second approach where an H-type grid was used. Its constantly good fineness along the vortex path, on one hand, causes a very high number of grid cells, even within secondary areas, on the other hand. As a compromise, a cylindrical ring is considered whose inner radius cuts the rotor blade.
Common to both procedures is the closed physical domain, which allows the vortex path to be completely covered for several rotations by the grid.

To examine the reliability of the Euler procedure several steady test calculations were performed, to which partly experimental data are available. Very good agreement was achieved. Small deviations for lifting cases can be related to the yet insufficient accuracy of the vortex path reproduction resulting in an inexact location of the vortex when impacting the following blade.

2. GOVERNING EQUATIONS AND SOLUTION ALGORITHM

In accordance with the flow field of the rotor the compressible Euler equations are formulated within a blade-attached cylindrical coordinate system which is rotating with the angular velocity $\vec{\omega}$ of the rotor (Fig. 1). This causes additional forces to be considered, i.e. the centrifugal and the Coriolis´ forces.

Hence, the Euler equations can be written in a differential, conservative formulation:

$$\vec{\Phi}_t + \frac{1}{r}\vec{E}_\varphi + \vec{F}_r + \vec{G}_z = -\vec{J} \ ,$$

with the solution vector $\vec{\Phi} = \begin{pmatrix} \rho \\ \rho u \\ \rho v \\ \rho w \\ e \end{pmatrix}$,

the spatial fluxes

$$\vec{E} = \begin{pmatrix} \rho u \\ \rho u^2 + p \\ \rho uv \\ \rho uw \\ \rho uH \end{pmatrix} , \qquad \vec{F} = \begin{pmatrix} \rho v \\ \rho vu \\ \rho v^2 + p \\ \rho vw \\ \rho vH \end{pmatrix} , \qquad \vec{G} = \begin{pmatrix} \rho w \\ \rho wu \\ \rho wv \\ \rho w^2 + p \\ \rho wH \end{pmatrix} ,$$

and the right-hand-side $\vec{J} = \frac{\rho}{r} \begin{pmatrix} v \\ 2(u-r\Omega)v \\ v^2 - (u-r\Omega)^2 \\ vw \\ v(H-r^2\Omega^2) \end{pmatrix}$.

Here $e = \frac{p}{\kappa - 1} + \rho \frac{q^2}{2}$ is the total energy per unit volume

and $H = \frac{e+p}{\rho}$ is the total enthalpy per unit mass.

The right-hand-side vector contains terms of the differentiation within the cylindrical coordinate system, and the centrifugal and Coriolis´ forces acting upon the control volumina due to the induced velocities.

Since the procedure is applied to body conforming, non-orthogonal grids, the system of equations is transformed into curvilinear, grid conforming coordinates. Exact details are given in [26,27].

Investigations have shown that it is irrelevant wether the velocity and the values that are directly influenced by it, the specific energy and enthalpy, are expressed in relative (i.e. blade-related) or in absolute (i.e. inertial) coordinates. Far more important is the fact, that all inter- and extrapolations applied during the iteration process are only performed with the absolute values, which are independent of the rotational velocity $r \cdot \Omega$, respectively the rotational energy $^1/_2 \cdot (r \cdot \Omega)^2$.
In case of a relative formulation the explicitly known value $r \cdot \Omega$ is added to the results of the inter- and extrapolations afterwards.
Beyond the absolute velocities, the rothalpy, with

$$\bar{h} = H - \frac{1}{2} (r \cdot \Omega)^2,$$

and derived from that, the roenergy, with

$$\bar{e} = e - \frac{\rho}{2} (r \cdot \Omega)^2$$

are introduced. Contrary to the enthalpy H the rothalpy $\bar{h}$ is constant within the area of a steady helicopter flow field.

The solution algorithm of the procedure presented is based on the EUFLEX-code of A. Eberle [28]. It is an explicit Finite-Volume-Scheme, in which the flow values are related to the cell-center points. The integration in time is first order accurate which is sufficient for the steady solution. The spatial derivatives are generally third order accurate and are switched down due to stability reasons to a lower order in the area of high flow gradients, such as e.g. in the shock region.
To solve the Riemann-problem, i.e. to evaluate the flow values at the cell face between two volumina, Eberle chose a Godunov-scheme [29]. Instead of a central mean of the values within the two neighbouring cells, as commonly used, an asymmetric average according to the method of characteristics and depending on the sign of the local eigenvalues is used.

This approach distinguishes itself by a small numerical dissipation and makes the otherwise commonly used additional application of artificial dissipation terms unnecessary. Herewith, one main reason for vortex diffusion is assumed to be diminished.
For a detailed explanation of the procedure see [28].

Presently, the algorithm is formulated in a timely explicit manner.

This allows an excellent degree of vectorization, however, it leads due the CFL-restriction to a high total computation time even when employing local time stepping. In the nearest future a change to an implicit formulation is planned especially due to the intended expansions to unsteady forward flight movement.

3. GRID STRUCTURES

The grid structures necessary for the Euler procedure are produced by an algorithm which finds its origin in an idea of Schwarz [27]. The grid points are found by solving Poisson's equation, whose source terms of the right-hand-side themselves are derived from Laplace's equation. This results in a system of three fourth order differential equations, decoupled in space, which is solved iteratively:

$$
\begin{aligned}
X_{\xi\xi} + X_{\eta\eta} + X_{\zeta\zeta} &= P \\
Y_{\xi\xi} + Y_{\eta\eta} + Y_{\zeta\zeta} &= Q \\
Z_{\xi\xi} + Z_{\eta\eta} + Z_{\zeta\zeta} &= R
\end{aligned}
$$

$$
\begin{aligned}
P_{\xi\xi} + P_{\eta\eta} + P_{\zeta\zeta} &= 0 \\
Q_{\xi\xi} + Q_{\eta\eta} + Q_{\zeta\zeta} &= 0 \\
R_{\xi\xi} + R_{\eta\eta} + R_{\zeta\zeta} &= 0
\end{aligned}
$$

Here, X,Y,Z represent either cartesian or cylindrical coordinates.

The procedure described above yields a very homogeneous distribution of grid points. However, to influence the local grid fineness, especially in the region of higher flow gradients, a series of mechanisms have been installed, which vary the grid at those critical points in a desired manner.

To reproduce the vortex convection without application of external wake models, the grids generated cover closed physical domains. Due to the symmetry in the hovering case the observation of only a part of the complete flow field, depending on the number of rotor blades is sufficient (Figs. 2,3). A periodic boundary condition is applied along the theoretical in- and outflow boundaries which employ a completely identical point distribution in order to avoid interpolations.

Two parallel ways were selected concerning the grid topologies. In one case an O-grid was chosen (Fig. 2), which has the great advantage that only a relatively small total number of points are needed to have a very good resolution in the blade's vicinity. Therefore, the complete rotor disk, including the wake, can be covered by the considered domain with an acceptable amount of storage requirements.
For helicopter rotors the tip vortex is of vital importance due to the interference with the following rotor blades. Therefore, a certain grid fineness is necessary along the vortex path in order to reproduce this effect physically correctly. The O-grid does not fulfill this requirement since the region between the blades is only roughly refined. This leads to a strong numerical dissipation, and therefore, to a diffusion of the vortex (Fig. 4). Nevertheless, this grid topology is useful for general studies because of low storage and time requirements.

During the investigations it was found that the size of the physical domain has a very significant influence towards the behaviour of the vortex with regards to its descent and contraction. A too small far-field distance, as visible e.g. in Fig. 2, obviously leads to a blockage of this movement, even under non-reflecting boundary conditions.

Thus, the outer boundaries were expanded 6 times to their original values (Fig. 5). In order to avoid a too great rise in the grid point number, and thus, in the computational expense the cell sizes increase very quickly towards the outside which has no negative effects within this region of negligible flow gradients. By this means, at a six times magnification of the physical domain the value of the computational domain was only increased by a factor of 1.7.

To avoid the disadvantages explained in connection with the O-grid, an H-grid (Fig. 3) was used for the second series of investigations. Since the H-structure is very point number intensive, the covered physical domain is confined to a cylindrical ring whose inner wall cuts the blade. At this boundary an additional condition must be chosen which will be explained in the next chapter. Fig. 3 shows, in comparison to the O-grid, a very acceptable point distribution at an area 90^0 behind the rotor blade. This fact is of advantage for the tip vortex convection.
Furthermore, the figure shows how the grid was expanded downwards in order not to prevent a descent of the vortex.
Presently, some work is perfomed in modifying the H-grid structure, in order to combine its advantages with those of the O-grid.

4. BOUNDARY CONDITIONS

The tangency condition at the rotor blade and a periodical boundary condition at the theoretical in- and outflow boundaries are used. At the far-field boundary a non-reflecting characteristic condition according to Eberle [28] is applied. This, however, still requires to attach the outer border of the grid at a very large distance to the blade thus avoiding disturbances of the vortex convection.

According to the limitation to a cylinder-ring for the H-grid an additional boundary condition at the inner boundary has to be introduced. Experiments with the O-grid have proved that across the whole length of the blade non-negligible radial velocities occur. Thus a 2-D condition does not apply. Several extrapolation algorithms were tested. The most qualified is obtained when setting

$$v^n = \begin{cases} \sqrt{q^2 - u^2 - w^2}\,, & \text{if} \quad q^2 - u^2 - w^2 \geq 0 \\ v^{n-1}, & \text{if} \quad q^2 - u^2 - w^2 < 0 \end{cases} .$$

Here the critical radial component is evaluated from the total velocity which limits the numerical radial flux diffusion.
Comparisons at a medium radial station with the method taking into account the complete rotor prove the efficiency of the boundary condition applied (Fig. 6).

5. RESULTS

The results presented in this paper were obtained for the H- and the O-grid using two different rotors. One of the rotors has an aspect ratio of 15 thus approximating a real system. The other one has an aspect ratio of 6 according to the model rotor studied by Caradonna and Tung [30]. Their pressure measurements were the basis to validate the algorithm.

For both rotors a non-twisted rectangular blade with a NACA 0012-profile was used.
Different numbers of blades were simulated by variation of the angle of aperture of the grid bodies.
In a further step the model rotor was modified by a twist and an altered blade tip geometry similar to that of the PF1-rotor of ONERA [13]. The results obtained were qualitatively correct.

The efficiency of the method to describe rotating flow on one hand and the numerical applicability of the periodical boundary condition on the other hand were proved by calculations performed with the non-lifting two-bladed model rotor. The results comply excellently with the measurements. Minimal deviations correspond to the influence of viscosity which is not taken into account (Fig. 7,upper row).

The agreement with measurements is still satisfactory when lift is produced. The deviations, however, are increased compared to the non-lifting case. Inclusion of the blade-vortex-interaction improves the results compared to the case of an isolated rotor blade exposed to the free stream significantly (Fig. 7, middle and lower row). This feature, however, is not yet exactly reproduced by the algorithm. Reasons for this deficiency are effects of diffusion caused by coarse grid structures and of an inaccurate representation of the vortex path.
A diagram of the c_p-distribution referred to the sound dynamic pressure along the blade radius shows the diminishing of the shock and herewith a reduction in blade loads when blade-vortex-interaction is included (Fig. 8).
The realistic rotor with $A = 15$ yielded similar results which are published elsewhere [11,12].

For the total pressure loss, respectively, the significant differences between a blade exposed to the free stream and a consideration of the blade-vortex-interactions are shown in the lower row of Fig. 8.
Severe losses in the area of the shock and at the origin of the tip vortex are displayed for the case of an isolated blade whereas in the second case a smaller total pressure loss is found due to a weaker shock. The vortex path can also be recognized in this case.

Figs. 9 and 10 show the results of some basic investigations on the principal properties of the algorithm.
In Fig. 9, two kinds of discretizising the physical domain were tested. In case a) a cylindrically shaped grid is applied as usual, whereas in case b) the grid is rectangular. Here the free stream velocity is increasing linearly along the radius as proposed e.g. by Stahl [9].
Both cases yield similar results for an isolated blade concerning the blade loads (Fig. 9a). The tip vortices, however, behave differently. In case a) the vortex path has an approximately circular shape. Thus, due to its curvature, at its inner side essentially larger velocities are generated than outside. This corresponds to the physical reality. In case b), however, the vortex leaves the trailing edge rectilinearly generating a pointsymmetrical velocity distribution (Fig. 9b).
Therefore, a model for the rotor flow of helicopters using a sheered translatoric free stream velocity profile is not suitable.

Fig. 10 shows the behaviour of the numerical wake leaving a fixed wing of low aspect ratio. As expected, the vortex sheet has descended and the vortex path is slightly inclined down- and inwards. Hence, the mechanisms acting upon the wake are reproduced in a qualitatively right manner by the Euler procedure and it is assumed that this holds true in the rotor case.

In Fig. 11 it is displayed to which extent the Euler equations principally apply to the problem of transporting inherent rotation through the considered domain. This was some years ago an open question.
In the upper sequence of pictures it is shown that in an H-grid, providing

a nearly constant distribution of points over different radial section cuts, the whole rotation is transported over the total range almost without loss. This is recognizable by the nearly unchanged magnitude of the induced velocities.
In the O-grid, however, the vortex carrying out one rotation passes subsequently very fine meshed, coarse and again fine meshed regions of the grid. Applying the same Euler algorithm as in the H-grid with the same amount of numerical dissipation, one can see the negative influence of the unsatisfactory discretization on the vortex consistency and location (Fig. 11, lower row).

These results lead to the conclusion that for the Euler method applied the exact description of the propagation of the vortex depends dominantly on the quality of the discretization chosen. Thus, the problem arises to match two opposite requirements: a very high degree of fineness in space over the complete flow field and simultaneously a moderate computational expense.

The problem is made even worse if the following results of a series of experiments are taken into account additionally. For an O-grid the influence of the far-field boundary was evaluated. The characteristic non-reflecting boundary condition itself was not changed. Fig. 12a shows the position of the vortex in the plane of symmetry. The outer boundary was located at 20 chords in radial direction and at 10 chords above and below the blade. The blade length itself was 15 chords.
The vortex hardly changed its position in vertical and radial direction, it almost seems to be blocked. Additionally only one single vortex can be recognized even after several rotations of the blade, and the downwash velocity distribution is unsatisfactory.
When the experimental conditions are varied by extending the physical domain to 120 chords in radial and vertical direction, it is found that the downwash velocities are qualitatively correcter and that the vortex moves with much less retainment. It lowers down, as expected, but, instead of contracting, moves outwards (Fig. 12b). This effect, also perceptible in Fig. 11, in the first moment seems to be opposite to reality. However, since the contraction of an upper vortex is known as a result of the velocities induced by the lower vortices, this contraction does not appear until the lower wake system has built up.
So, what can be seen in Fig. 12b is a starting situation, which in reality changes after a certain number of blade revolutions.
The same effects are in principle found using a simple low order procedure, as e.g. a vortex-lattice-method. At the beginning, the tip vortex moves outwards, being forced to contract not before enough vortex loops have developed beneath.

Now, the question is arising, wether the Euler procedure is actually capable to reproduce more than one vortex ring, especially since only one loop could be recognized in the figures described before. This fact was investigated by examining planar cuts through the grid at different constant azimuth angles.
Actually two systems of tip vortices are recognized in a certain range behind the rotor blade, one of them being diffused due to the problems of the O-grid discussed before (Fig. 13). In regions of coarse mesh structures, however, they are forced to merge into each other. Under this circumstances, no further vortex loops can be expected. Thus, the requirement discussed above to use a constantly fine meshed grid is again confirmed. Additionally, deliberations are made, deviating from the original intentions, to use a simple far wake system to overcome the starting phase.

Fig. 14 displays a calculation on the model rotor of Caradonna and Tung fitted with a modified tip geometry, compared with the results of the original model rotor. The free stream conditions were given with $M_{tip} = 0.815$ at a collective pitch angle of $\Theta_c = 5^0$. In the modified case, a twist of -2^0

was chosen, decreasing the local angle of attack to only 3^0 at the tip.
The tip of the blade was designed similar to that of the PF1-rotor of ONERA [13], however, a NACA 0012 - profile was used.
Since no experimental data exist for this case only a qualitative interpretation is possible. Decreased low pressure and the avoidance of the supersonic area are the result of a smaller local geometrical angle of attack and of the swept leading edge.
Further numerical experiments will be carried out when the results are comparable with measurements.

6. CONCLUSIONS

A method is presented basing on the solution of the Euler equations to calculate the steady flow around the rotor of a helicopter taking blade-vortex-interference implicitly into account.
It is shown, that the Euler equations applying a procedure of minor dissipation are capable of transporting a rotation involved within the flow field without remarkable losses. It has to be provided, however, that the computational grids are sufficiently fine meshed and that the resolution hardly varies over the whole range of vortex convection.
Furthermore, care has to be taken that the distance of the far-field boundary to the blade is sufficiently large to avoid blocking of the vortex propagation.
Both conditions imply that a large computer storage is required which has to be encountered by a suitable choice of the grid.
The results obtained are in good accordance to the experimental data although the requirements discussed above are not yet implemented optimally. Therefore, some deviations in the description of the vortex convection are found, leading to a still inaccurate representation of the flow conditions at the following rotor blade.

7. ACKNOWLEDGEMENT

The paper is partly based on research work funded until the end of 1987 by the Bundesministerium für Forschung und Technologie BMFT (Ministry of Research and Technology).

8. REFERENCES

[1] Roberts, T.W., Murman, E.M.: Solution Method for a Hovering Rotor Using the Euler Equations
AIAA-Paper 85-0436, 1985

[2] Roberts, T.W., Murman, E.M.: Euler Solutions for the Flow Around a Hovering Helicopter Rotor
AIAA Paper 86-1784, 1986

[3] Sankar, N.L., Wake, B.E., Lekoudis, S.G.: Solution of the Unsteady Euler Equations for Fixed and Rotor Wing Configurations
AIAA Paper 85-0120, 1985

[4] Sankar, N.L., Tung, C.: Euler Calculations for Rotor Configurations in Unsteady Forward Flight
Proceedings of the 42nd Annual Meeting of the American Helicopter

Society, Washington,D.C., 1986

[5] Wake, B.E., Sankar, N.L., Lekoudis, S.G.: Computation of Rotor Blade Flows Using the Euler Equations
J. Aircraft, Vol. 23, No. 7, 1986, pp. 582-588

[6] Agarwal, R.K., Deese, J.E.: Euler Calculations for Flowfield of a Helicopter Rotor in Hover
AIAA Paper 86-1782, 1986

[7] Chang, I-C., Tung, C.: Euler Solution of the Transonic Flow for a Helicopter Rotor
AIAA Paper 87-0523, 1987

[8] McCroskey, W.J.: Some Rotorcraft Applications of Computational Fluid Dynamics
Second International Conference on Rotorcraft Basic Research, College Park, Maryland, Feb. 1988

[9] Stahl, H.: Application of a 3D Euler Code to Transonic Blade Tip Flow
12th European Rotorcraft Forum, Garmisch-Partenkirchen, 1986, Paper-No. 29

[10] Kroll, N.: Computation of the Flow Fields of Propellers and Hovering Rotors Using Euler Equations
12th European Rotorcraft Forum, Garmisch-Partenkirchen, 1986, Paper-No. 28

[11] Krämer, E., Hertel J., Wagner, S.: Computation of Subsonic and Transonic Helicopter Rotor Flow Using Euler Equations
13th European Rotorcraft Forum, Arles, France, 1987, Paper No. 2-14

[12] Hertel, J., Krämer, E., Wagner, S.: Euler Solutions for Steady Flow of a Helicopter Rotor
Second International Conference on Rotorcraft Basic Research, College Park, Maryland, USA, Feb. 1988

[13] Desopper, A., Lafon, P., Philippe, J.J., Prieur, J.: Effect on an Anhedral Swept-back Tip on the Perfomance of a Helicopter Rotor
13th European Rotorcraft Forum, Arles, France, 1987, Paper No. 2-4

[14] Caradonna, F.X., Tung, C.: Finite-Difference Computation of Rotor Loads
International Conference on Rotorcraft Basic Research, Research Triangle Park, N. Carolina, Feb. 1985

[15] Strawn, R.C., Caradonna, F.X.: Conservative Full-Potential Model for Unsteady Transonic Rotor Flow
AIAA-Journal, Vol. 25, No. 2, Feb. 1987, pp. 193-198

[16] Tung, C., Caradonna, F.X., Boxwell, D.A., Johnson, W.R.: The Prediction of Transonic Flow on Advancing Rotors
Proceedings of the 40th Annual National Forum of the American Helicopter Society, Washington, D.C. 1984

[17] Caradonna, F.X., Tung, C., Desopper, A.: Finite-Difference Modelling of Rotor Flows Including Wake Effects
Journal of the American Helicopter Society, Vol. 29, April 1984, pp. 26-33

[18] Chang, I-C.: Transonic Flow Analysis for Rotors Part I: Three-Dimensional, Quasi-Steady, Full-Potential Calculation
NASA TP-2375, 1984

[19] Chang, I-C.: Transonic Flow Analysis for Rotors Part II: Three-Dimensional, Unsteady, Full-Potential Calculation
NASA TP-2375, 1985

[20] Tung, C., Chang, I-C.: Rotor Transonic Computation with Wake Effect
4th International Conference on Applied Numerical Modeling,
Taiwan, Rep. of China, Dec. 1984

[21] Chang, I-C., Tung, C.: Numerical Solution of the Full-Potential Equation for Rotors and Oblique Wings Using a New Wake Model
AIAA-Paper 85-0268, Jan. 1985

[22] Sankar, N.L., Prichard, D.: Solution of Transonic Flow Past Rotor Blades Using the Conservative Full-Potential Equation,
AIAA-Paper 85-5012, Oct. 1985

[23] Egolfe, A., Sparks, P.: Hover Rotor Airload Predictions Using a Full Potential Flow Analysis with a Realistic Wake Geometry
Proceedings of the 41st Annual National Forum of the American Helicopter Society, Ft. Worth, TX, 1985

[24] Tauber, M.E., Owen, F.K., Langhi, R.G., Palmer, G.E.: Comparison of Calculated and Measured Velocities Near the Tip of a Model Rotor Blade at Transonic Speeds
NASA TM 86697, 1985

[25] Strawn, R.C., Caradonna, F.X.: Numerical Modeling of Rotor Flows with a Conservative Form of the Full-Potential Equations
AIAA-Paper 86-0079, Jan. 1986

[26] Thompson, J.F., Warsi, Z.U.A., Mastin, G.W.: Numerical Grid Generation
North - Holland, New York, 1985

[27] Schwarz, W.: Dreidimensionale Netzgenerierung für ein Finites Volumen-verfahren
MBB/LKE122/S/PUB/206, 1985

[28] Eberle, A.: A New Flux Extrapolation Scheme Solving the Euler Equations for Arbitrary 3-D Geometry and Speed
MBB-EUFLEX MBB/LKE122/S/PUB/140, 1984

[29] Godunov, S.K.: A Finite Difference Method for the Numerical Computation of Discontinuous Solutions of the Equations of Fluid Dynamics
Math. Sb. Vol.47, pp. 357-93, 1957

[30] Caradonna, F.X., Tung, C.: Experimental and Analytical Studies of a Model Helicopter Rotor in Hover
NASA TM-81232, 1981

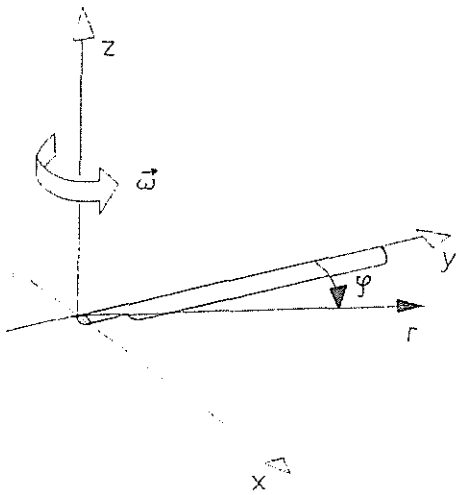

FIG. 1 : Blade-attached coordinate system

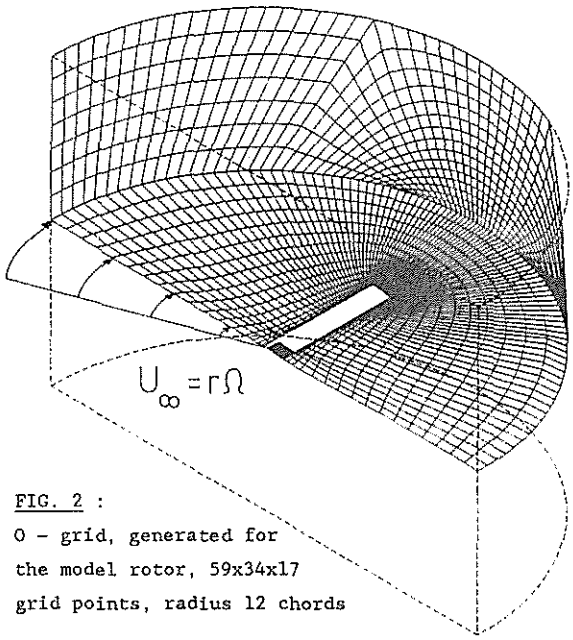

FIG. 2 :
O - grid, generated for
the model rotor, 59x34x17
grid points, radius 12 chords

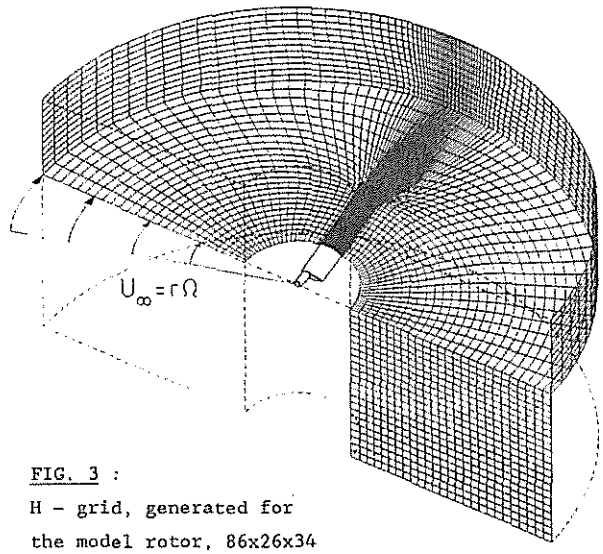

FIG. 3 :
H - grid, generated for
the model rotor, 86x26x34
grid points, inner boundary at r/R = 0.4,
outer boundary at r/R = 2., grid extended downwards

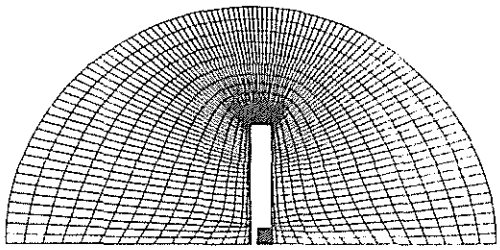

FIG. 4 : Discretization of the rotor disk (O - grid)

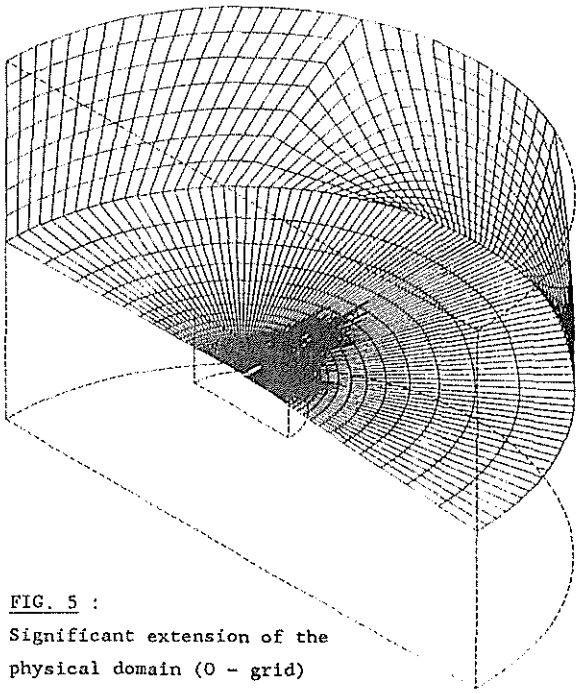

FIG. 5 :
Significant extension of the
physical domain (O - grid)

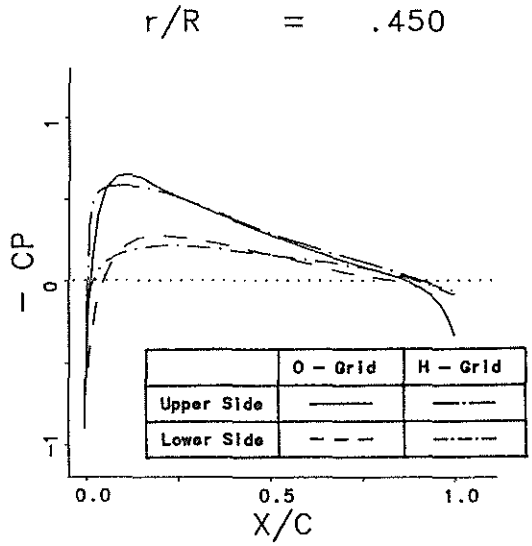

FIG. 6 : Validation of the inner boundary
condition of the H - grid

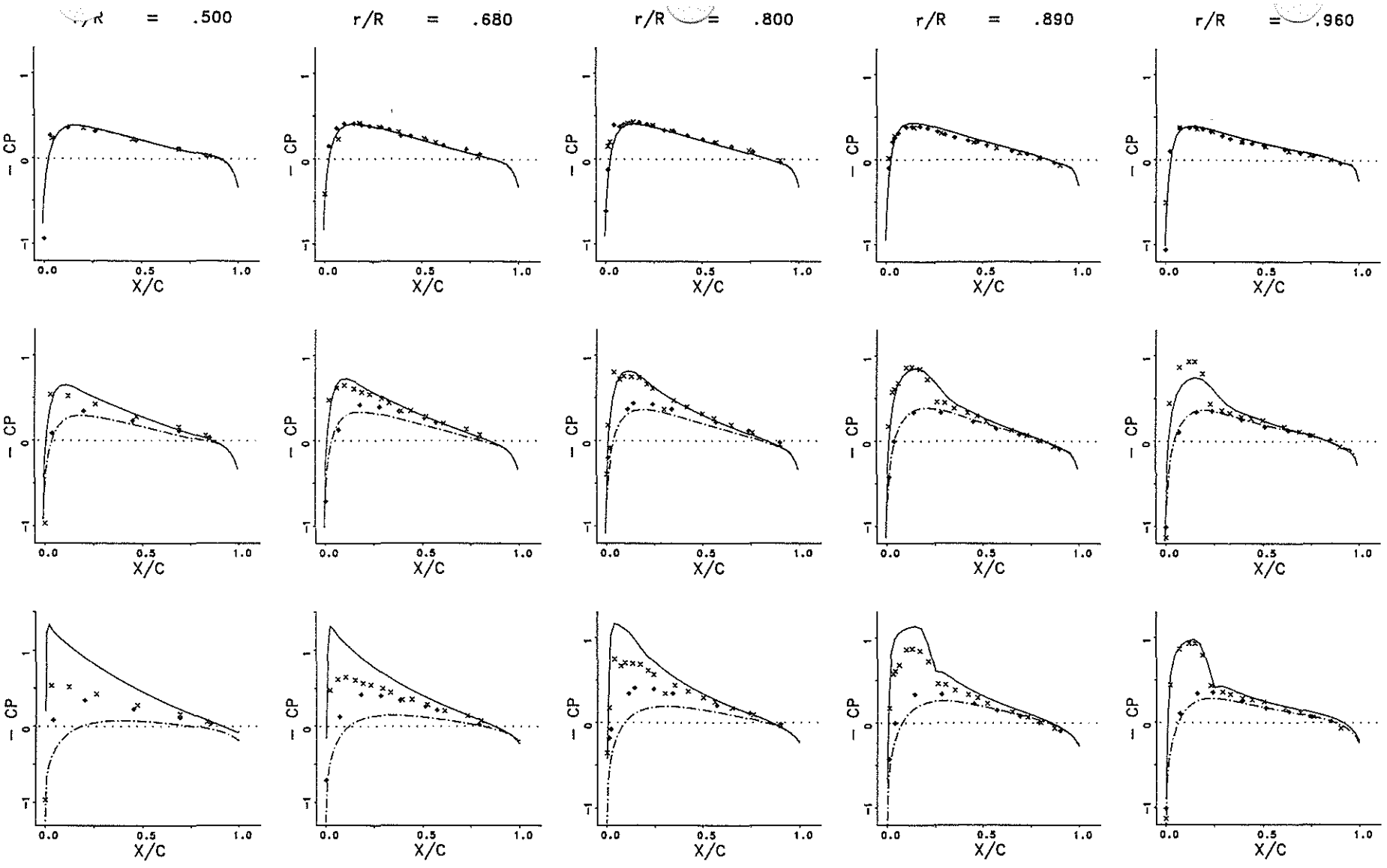

	Experiment	Theory
Upper Side	×	———
Lower Side	◆	—·—·—

FIG. 7 : Pressure distribution for the model rotor. Comparison of the results with measurements

upper row : $M_{tip} = 0.52$, $\theta_c = 0°$

middle row : $M_{tip} = 0.815$, $\theta_c = 5°$ consideration of the blade-vortex-interaction

lower row : $M_{tip} = 0.815$, $\theta_c = 5°$ isolated rotor blade

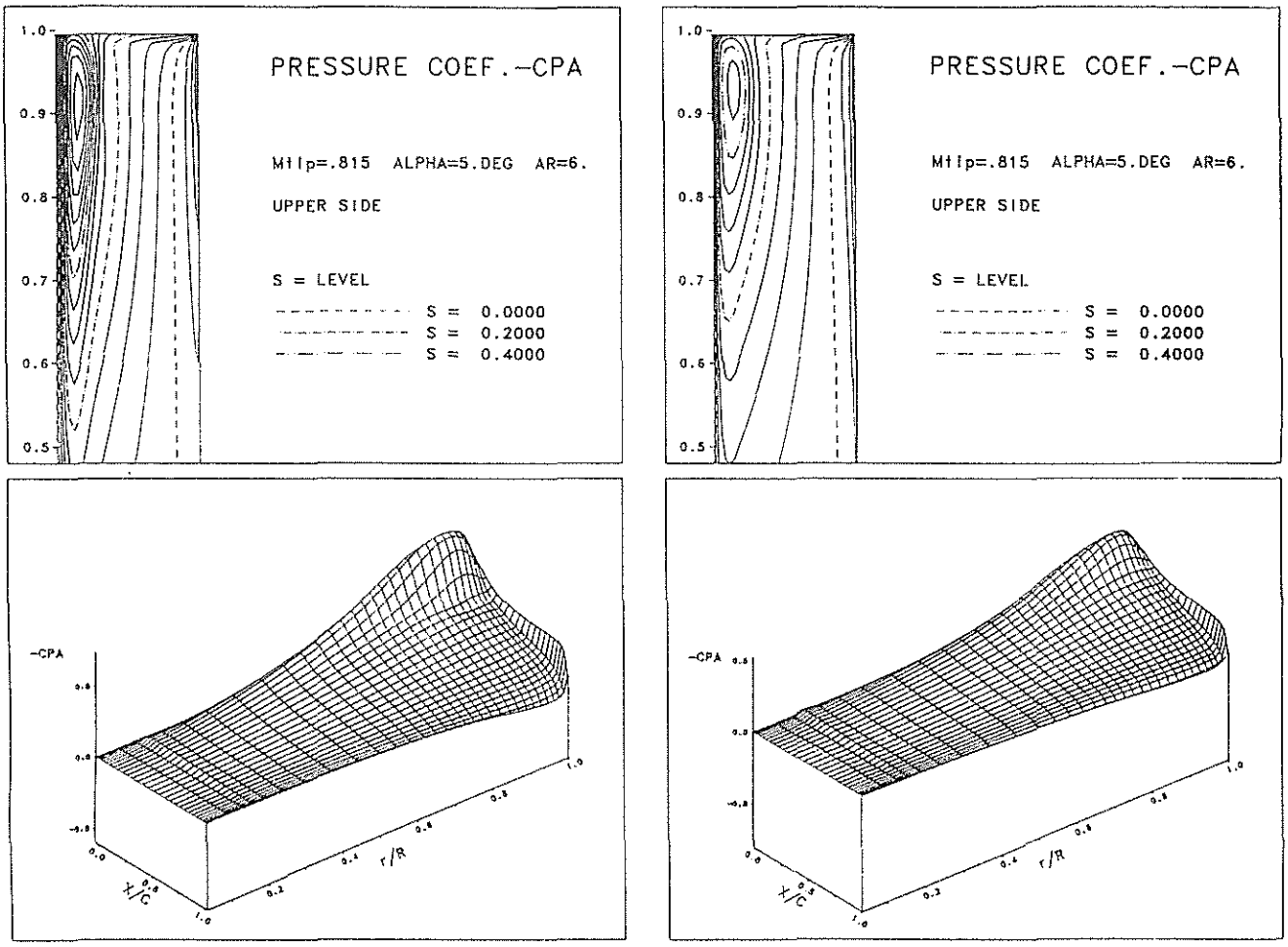

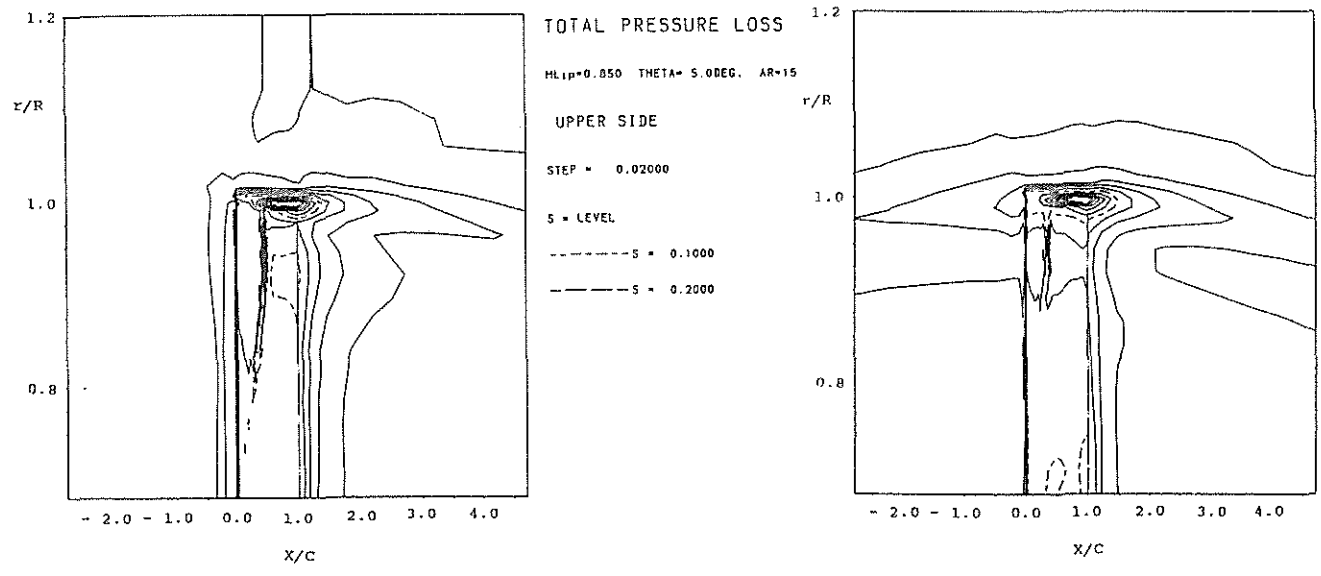

Isolated Rotorblade

Consideration of the Blade-Vortex-Interaction

FIG. 8 : Comparison of pressure distributions and total pressure losses for a rotor blade with and without consid n of the blade-vortex-interaction

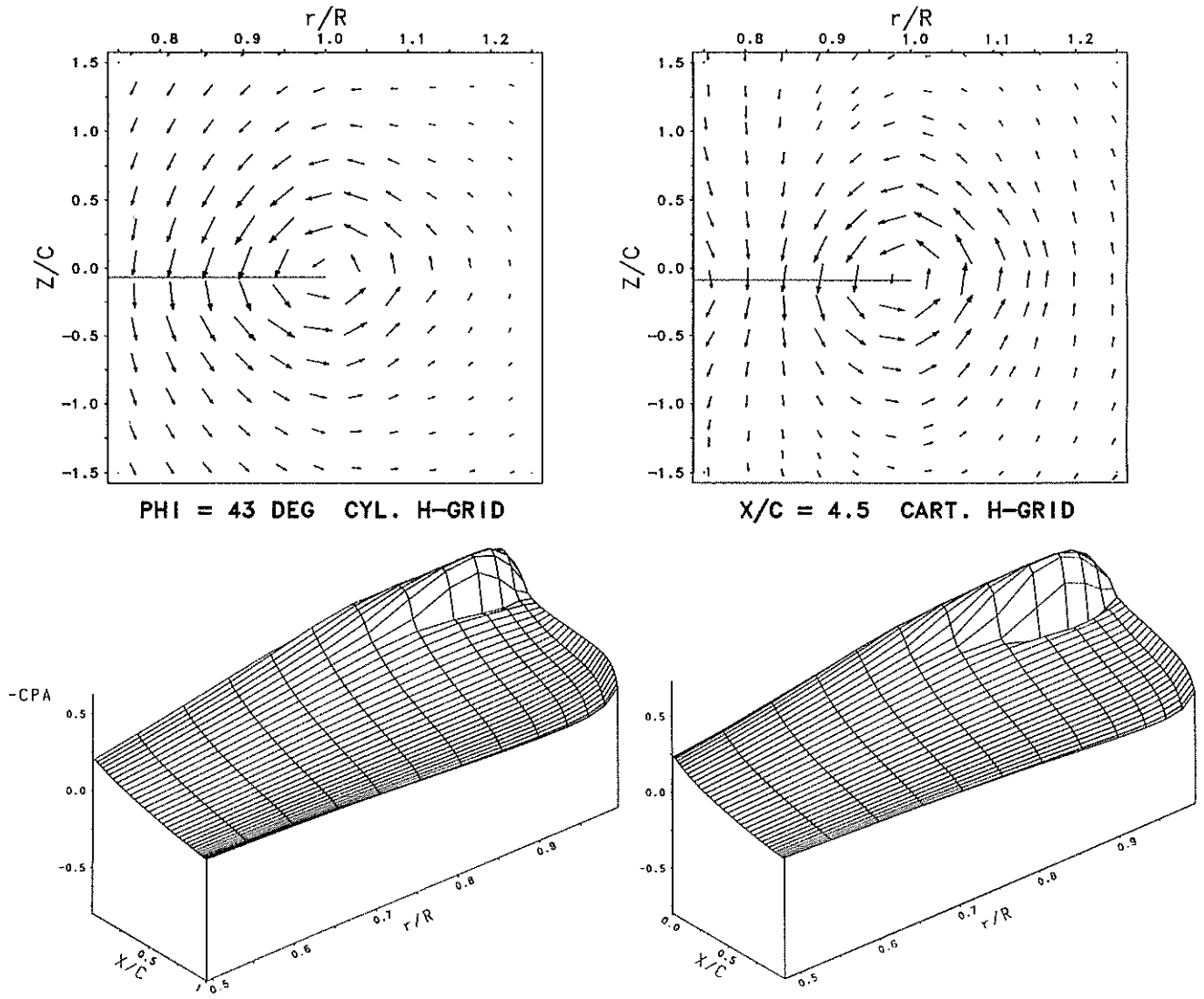

FIG. 9 : Comparison of the tip vortex structure and the pressure distributions for an isolated rotor blade using a bended, cylindrically shaped and a cuboidal, cartesian H - grid

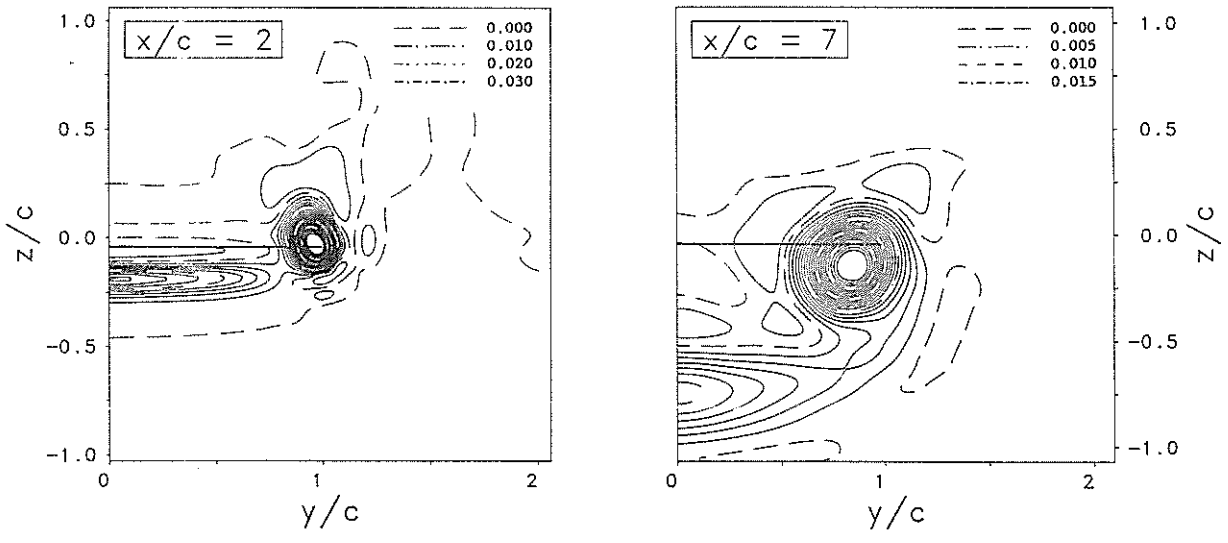

FIG. 10 : Tip vortex contraction and descent for a fixed wing of low aspect ratio

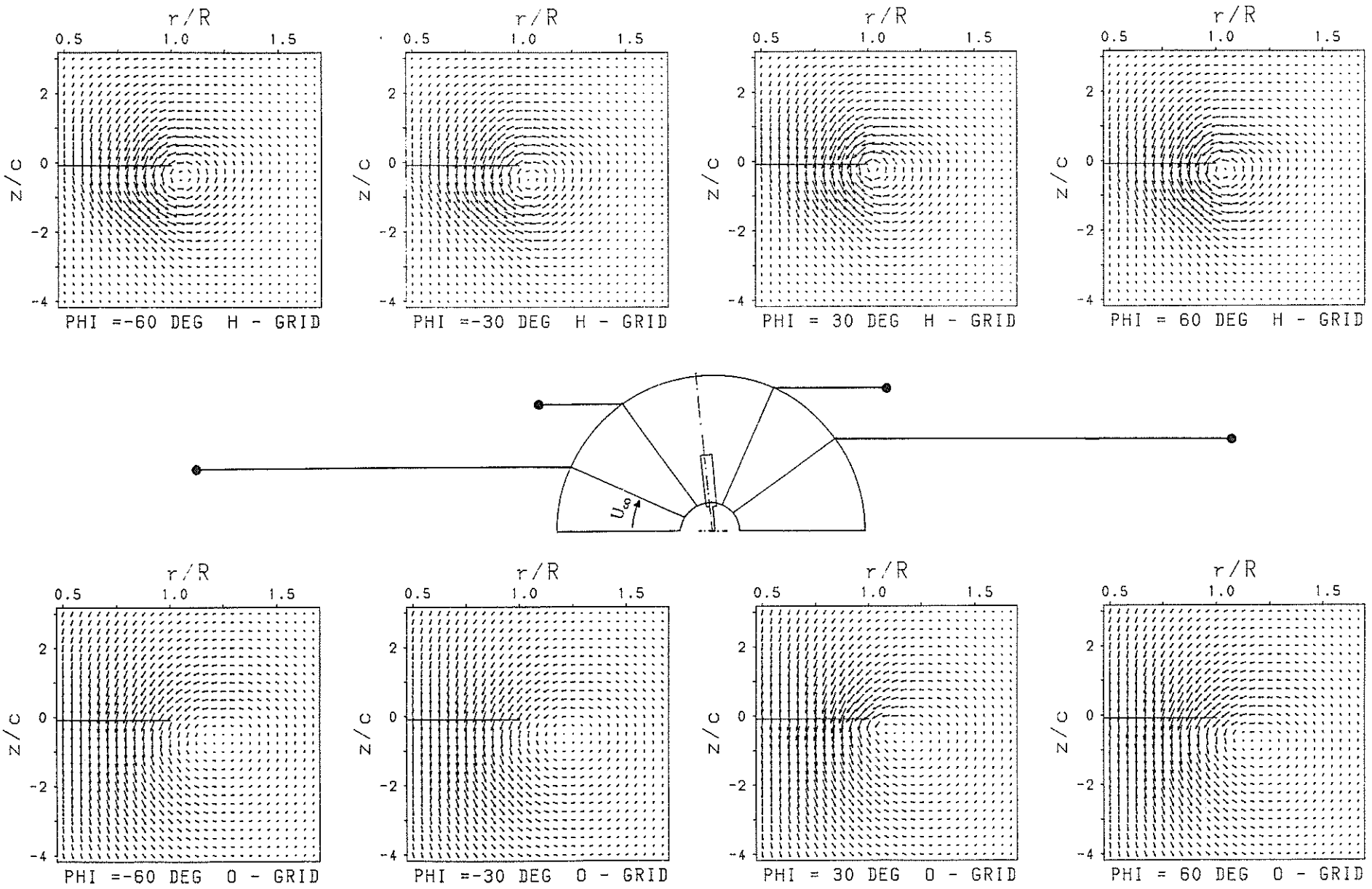

FIG. 11 : Behaviour of the vortex convection in an H - grid with low diffusion (upper row) and an O - grid with great diffusion (lower row)

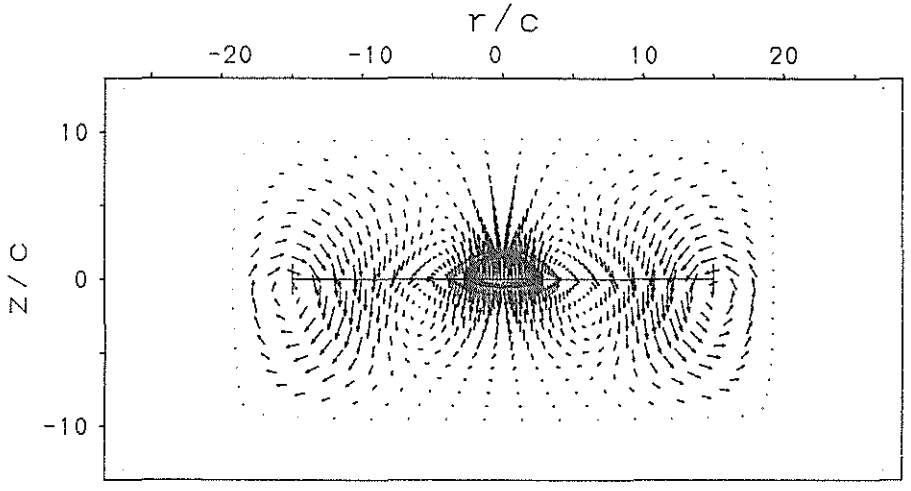

a) SMALL DISTANCE OF FAR-FIELD BOUNDARY (R = 20)

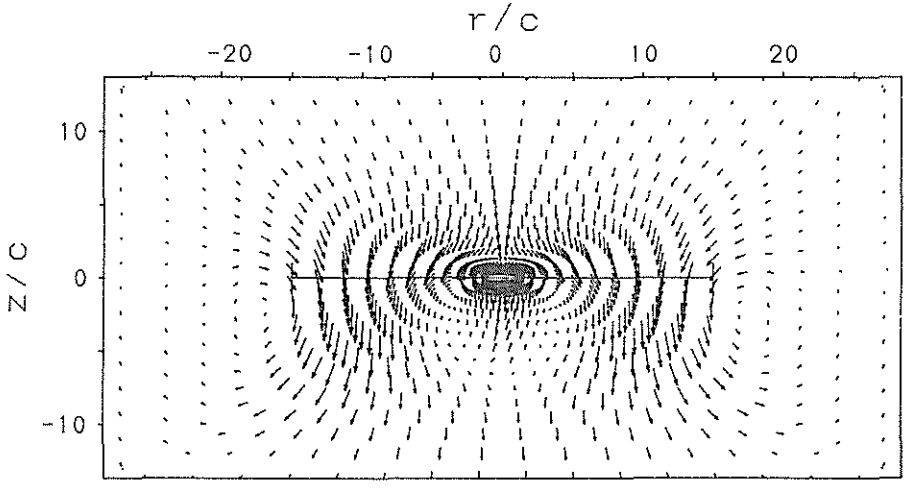

b) GREAT DISTANCE OF FAR-FIELD BOUNDARY(R = 120)

FIG. 12 : Influence of the distance of the far-field boundary on the tip vortex convection

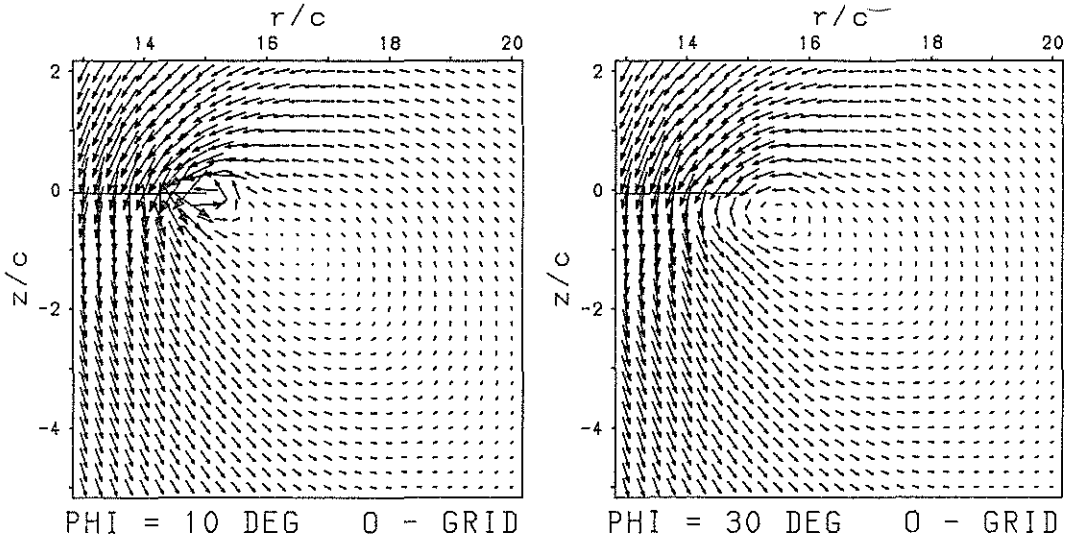

FIG. 13 : Fusing of two discrete vortices to a single one as a consequence of coarse structures in an 0 - grid

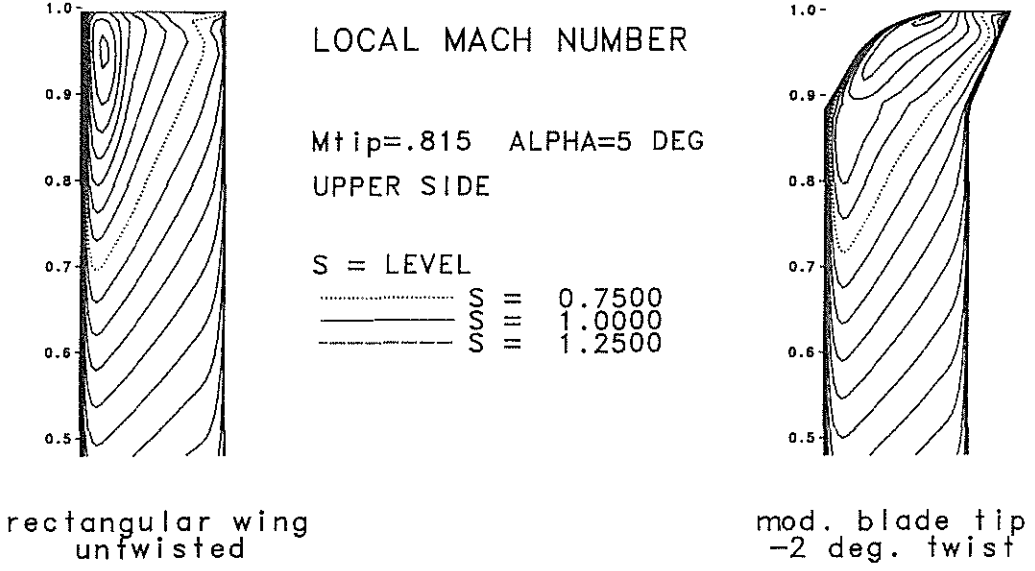

FIG. 14 : Comparison of a calculation for a conventional and for a modified blade tip geometry with an additional twist of the rotor blade